DOI 10.1007/s11106-022-00306-9
Powder Metallurgy and Metal Ceramics, Vol. 61, Nos. 3-4, July, 2022 (Russian Original Vol. 61, Nos. 3-4, March-April, 2022)

3D PRINTING OF IRON-BASED LATTICE STRUCTURES PRODUCED BY SELECTIVE LASER MELTING

A.V. Minitskyi,[1,2] O.V. Stepanov,[1] S.V. Radchuk,[1] Ye.G. Byba,[1] and P.I. Loboda[1]

UDC 621.762, 629.78

The mechanical properties of lattice structures with 78–79% pore volume produced from iron powders by selective laser melting were studied. As the mechanical properties of lattice structures can be predicted from the topology and dimensions of the unit cell, the influence of spatial orientation of the unit cells on the mechanism whereby the samples are deformed should be also established. Three types of lattice structures with different spatial orientation of unit cells represented by simple cubic volumes of porous material with the same size of lattice and unit cell generatrixes were considered. The response of the lattice structure to different types of loads was analyzed. Measurements of the elastic modulus in four-point bending tests showed that porous 3D lattices with different unit cells had an elastic modulus of the same order, from 17.2 to 23.9 GPa. Compression tests of the 3D lattice structures indicated that the lattices located at an angle of 45° to the z axis deformed according to similar patterns and had almost the same yield stress (14.0–15.4 MPa). The highest yield stress (40.5 ± 3.3 MPa) was observed in the lattices whose unit cells were parallel to the x, y, and z axes, which is due to the layered deformation of the cells. The greatest impact toughness (22.1–23.2 J/cm^2), as well as the compressive yield stress and elastic modulus, was also shown by these lattices. Analysis of the fracture structure of the samples after impact toughness tests indicated that the iron lattice structures of all three types had pit microrelief characteristic of viscous fracture. The results demonstrated the prospects of applying additive manufacturing techniques for the development of iron-based powder materials by selective laser melting to form a lattice structure with highly reproducible mechanical characteristics.

Keywords: *additive manufacturing, selective laser melting, lattice structures, iron powder, 3D printing, unit cell.*

INTRODUCTION

In recent years, additive manufacturing (AM) processes have found wide application as they allow the fabrication of complex parts, reduce the number of operations, and decrease the net cost of precision products [1–3]. Selective laser melting (SLM) is one of the most common 3D printing methods [4–6]. This process produces articles of different configuration and, importantly, of different internal pore channel system, providing for the development of lattice structures [7, 8].

Lattice structures are becoming increasingly popular in engineering because they find a wide range of applications, including protective structures, heat exchangers, orthopedic implants, and vibration absorbers [9].

[1]National Technical University 'Igor Sikorsky Kyiv Polytechnic Institute, Kyiv, Ukraine.
[2]To whom correspondence should be addressed; e-mail: minitsky@i.ua.

Translated from Poroshkova Metallurgiya, Vol. 61, Nos. 3–4 (544), pp. 70–80, 2022. Original article submitted March 31, 2022.

Gibson and Ashby [10] were among the first to describe in detail the application of additive manufacturing processes to develop lattice structures. Lattice structures that consist of continuous bars or lamellas formed by cell edges and faces are used as structural materials in mechanisms to which weight reduction requirements are applied. The lattice mechanical properties depend not only on the powder material and printing quality but also on the geometry of structural components [11].

The paper [12] examined the deformation of stainless-steel lattice structures. Relative density and topology of unit cells, which determine the height of the stress–strain curve and structural fracture mechanism, turned out to be two basic parameters characterizing the mechanical behavior of such structures. It was pointed out that imperfect lattice surface could not ensure stable results in the case of shear strains, and high reproducibility of the mechanical characteristics was observed only when lattices were tested by compression.

An analytical model was developed in [13] to describe variation in the elastic modulus and initial compressive strength in multilayer lattice structures shaped as bcc unit cells. Layer-by-layer fracture mechanism was revealed for such structures. Hence, the effect from the number of layers and cells on the deformation mode and fracture mechanism was studied.

The paper [14] examined the mechanical compressive properties of samples with lattice structures with two bcc cell types: simple cells and cells with an additional stiffening rib along the z axis. The effect from sizes of lattice components and cells on the deformation was found. The unit cell size was shown to be the main factor that influenced the deformation and fracture mechanism for the samples.

One of the recent papers on lattice structures paid significant attention to the search of the optimal cell topology that would promote the best mechanical properties at the lowest amount of the material and the maximum ratio between stiffness/strength and weight [15]. The unit cell topology, relative density, and structure were shown to play an important role in determining the mechanical properties of lattice structures fabricated by selective laser melting. A simple cubic lattice has the highest compressive strength among all the lattice structures analyzed.

Analysis of the publications demonstrated that a simple cubic lattice was most promising topology for unit cells. However, the important factor such as angles at which the unit cells are oriented in the space of lattice structures was not determined. To understand the interrelation between the location of unit cells of set size and topology and the mechanical properties is a necessary condition for the development of metal structures with excellent mechanical properties. Considering that iron and steel remain the main structural materials as they have high mechanical properties and low cost, the mechanical properties of lattice structures produced from iron powders by selective laser melting should be examined. Such structures can be used as protective components with low specific weight and thus promote high deformation energy for military equipment.

The objective is to study how the spatial orientation of a cubic unit cell influences the mechanical properties of lattice structures produced form iron powders by selective laser melting.

EXPERIMENTAL PROCEDURE

Lattice structures with 78–79% total pore volume were produced by selective laser melting (SLM) with a Realizer SLM50 3D printer (Realizer, Germany) using the SOLIDWORKS software. The atomized spherical PZhR3 iron powder of –63+45 μm size fraction was used for printing. The powder had the following chemical composition, wt.%: Fe matrix, 0.05 C, 0.08 Si, 0.20 Mn, 0.02 S, 0.02 P, and 0.2 O. The layer thickness was 70 μm. The laser power was 75 W at a scan rate of 0.4 m/sec, which corresponds to a distance of 20 μm between the processing points and an exposure time at one point of 50 μsec [16].

To plot a microstrain curve with data of four-point bending testing, a Ceramtest machine was employed (Gobor LLC, Ukraine) with automatic computer recording of experimental data. The distance between the external supports was 40 mm and that between the internal ones was 20 mm. A highly sensitive displacement sensor (sensitivity not lower than $2 \cdot 10^{-7}$ m) was fixed between the middle rolls to record the deformation with an accuracy of 10^{-5}. The beam moved at a rate of 0.2 mm/min. The Ceramtest machine was equipped with an automated control and data processing system, allowing the elastic modulus, strength, and ductility to be determined with an accuracy of no less than 2%.

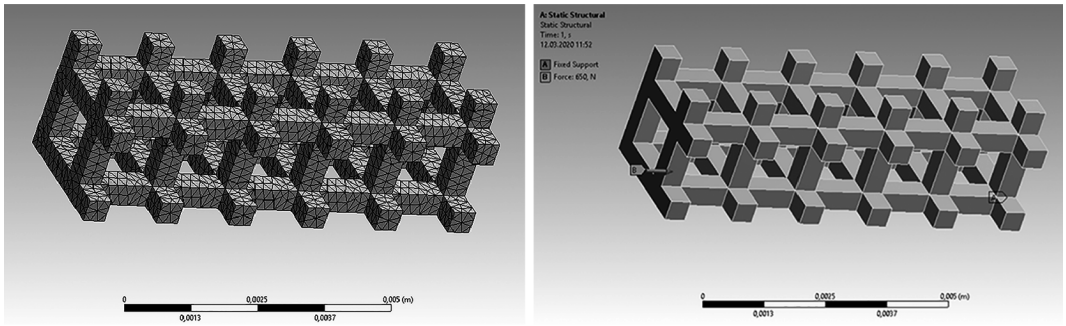

a *b*

Fig. 1. Nodal distribution of the lattice structure in the ANSYS software package (*a*) and boundary conditions and symmetry conditions (*b*)

Impact toughness tests of 3D lattice structures were performed using a KM-5 pendulum machine (Asma-Prylad, Ukraine), which complies with ISO 148 requirements through DSTU 3669–97.

Metallographic analysis was carried out with a REM-106I scanning electron microscope (Selmi, Ukraine).

The deformation of lattice structures was modeled by finite-element simulation with the ANSYS 19R1 Academic Edition applied software package [17].

The development of a 3D lattice model with the ANSYS19R1 system ensures correct analysis of the mechanical properties and stress–strain state of the materials for parallel-sided planes. The inverse finite-element problem is one of the most common methods for determining effective or homogenized properties of inhomogeneous materials [18]. In contrast to the direct problem, which is intended to analyze the spatial distribution of strain and stress fields and their division into normal and shear strains and stresses, the inverse problem is aimed at assessing the effective properties of the structure from its response to the load applied.

A representative volume was used as a lattice structure model (Fig. 1*a*). Parameters of the 3D lattice structure of iron with parallel unit cells were assigned as a simple cube.

Boundary conditions and symmetry conditions A, fixed plane B (Dirichlet boundary conditions), and load C (Neumann boundary conditions) were applied (Fig. 1*b*). The force load on one of the planes (z = 8.2 mm) was oriented in the lattice compression direction. The opposite plane (z = 0) was fixed (Δx, Δy, and Δz = 0 for all plane points). The symmetry condition was imposed along the normal line to the surface on the section (denoted by x).

DISCUSSION OF RESULTS

The calculations resulted in a field of displacements (u, v, w) and total displacement (Fig. 2).

The response of parallel unit cells to different loads was analyzed. For each of the loads, maximum displacements were calculated along the load axis (such displacements are observed on the plane to which the load was applied). The dependence of displacements (w) on loads applied (F) is shown in Fig. 3.

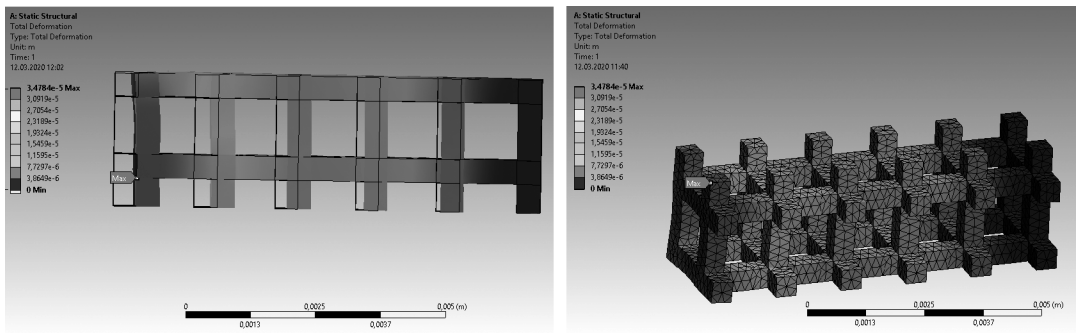

a *b*

Fig. 2. Deformed model as compared to the initial sizes (*a*) and total deformation of the model (*b*)

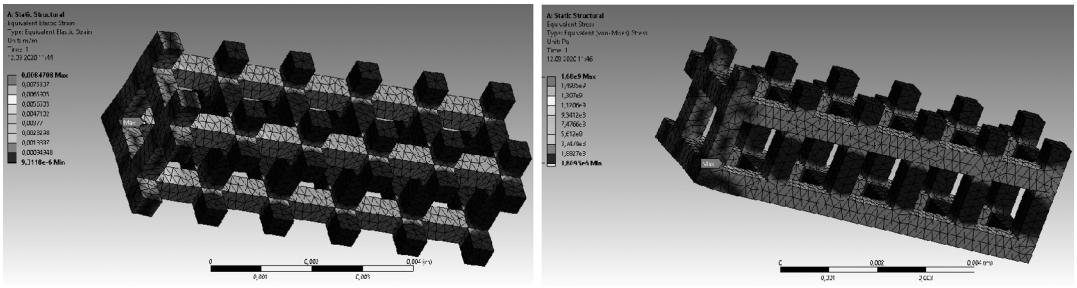

a *b*

Fig. 3. Strain field (*a*) and stress field (*b*)

Let us calculate the effective area of the element as

$$S_{\text{eff}} = a \cdot b = 2.55 \cdot 2.55 = 6.5025 \text{ mm}^2$$

and strain as

$$\varepsilon_{\text{ff}} = w/l,$$

where w is the maximum displacement in the load direction (z axis) and l is the size of the element along the z axis before deformation.

The effective elastic modulus is calculated as

$$E_{\text{eff}} = F / (S_{\text{eff}} \cdot \varepsilon_{\text{eff}}).$$

The model calculations indicated that the effective elastic modulus, according to the stress–strain curve (Fig. 4), is 23.5 GPa.

For experimental assessment of the mechanical properties of lattice iron structures, three types of lattices with different spatial orientation of unit cells as simple cubes in a porous material were 3D-printed (Fig. 5). Hence, lattice 1 has unit cells oriented at 45° to the x, y, and z axes; lattice 2 has simple cubes parallel to the x, y, and z axes (identically to the 3D model); and lattice 3 has unit cells parallel to the y axis and located at 45° to the x and z axes (Fig. 6).

In the development of a printing model, the average sizes of cell generatrixes, which differ from each other only by the orientation of unit cells as simple cubes in the lattice, were set; this was taken into account in the study of their mechanical properties. To confirm the sizes of lattice elements and unit cells, lattice structure images were subjected to computer processing. The calculation results showed that the average sizes of cell generatrixes correspond to 420–530 μm and the average sizes of cells to 1100–1250 μm (Table 1).

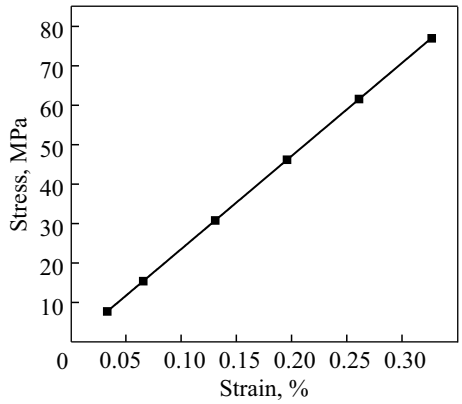

Fig. 4. Stress–strain curve for the 3D model

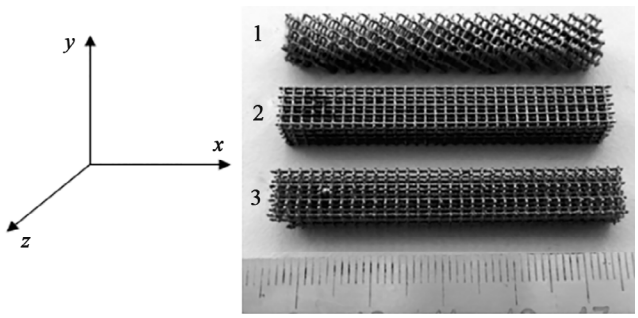

Fig. 5. Images of SLM-printed lattices

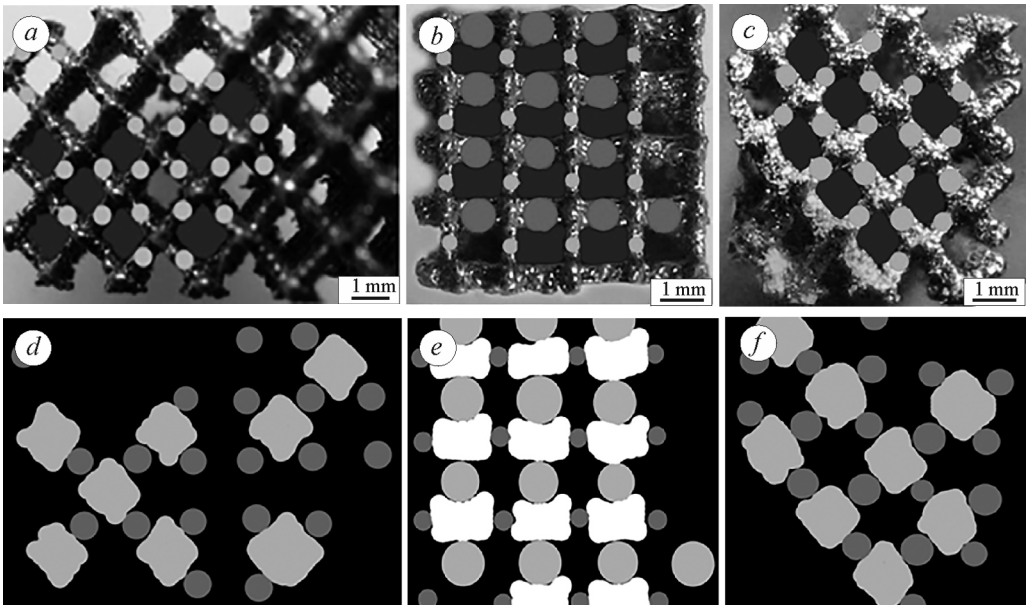

Fig. 6. Unit cells as simple cubes in the graphics editor after limitation of the measurement areas (*a–c*) and image computer processing (*d–f*): *a*, *d)* lattice 1; *b*, *e)* lattice 2; *c*, *f)* lattice 3

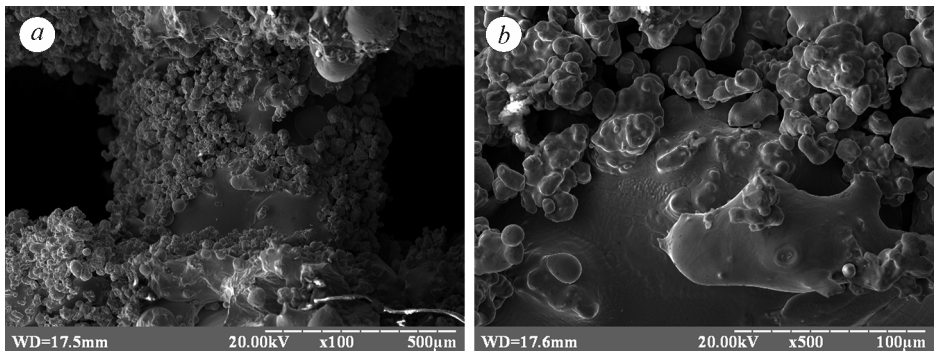

a *b*

Fig. 7. Microstructure of a 3D lattice sample

Microscopy analysis indicated that the lattice microstructure typical of all lattice structures consisted of an internal continuous framework formed in the melting of iron particles and located on the surface of spheroidized powder particles (Fig. 7).

Testing of 3D lattices by three- and four-point bending demonstrated that support rolls ‘squeeze’ into the lattice but internal cells do not fail under the impression and the connections are strong and deform plastically (Fig. 8). In the first deformation stage, a linear region, characterizing the direct proportionality between the stress and strain, is observed on the load curve. Accordingly, the elastic moduli were found in the elastic region using four-point bending data (Table 2). The measurement results showed that the 3D lattices had elastic moduli of one order of magnitude: from 17.2 to 23.9 GPa.

TABLE 1. Sizes of SLM-Printed Lattices

Type of lattice	Lattice generatrixes, µm	Cell sizes, µm
1	430–560	1100–1230
2	400–470	1090–1260
3	420–530	1090–1270

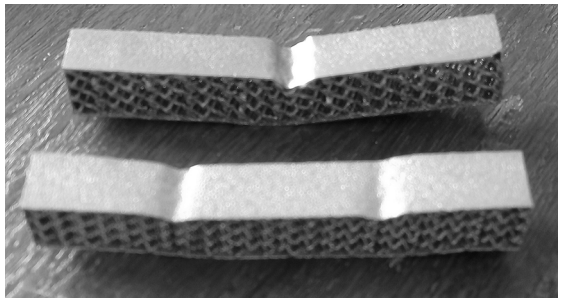

Fig. 8. 3D lattice samples tested by three- and four-point bending

TABLE 2. Mechanical Properties of 3D Lattice Structures of Different Types

Type of lattice	Elastic limit σ_{001}, MPa	Yield stress σ_{02}, MPa	Elastic modulus E, GPa	Impact toughness KCB, J/cm^2
1	11.6 ± 1.2	14.0 ± 1.5	20.0 ± 0.5	13.5 ± 0.8
2	35.5 ± 3.3	40.5 ± 3.3	23.9 ± 0.5	23.2 ± 1.3
3	13.9 ± 1.5	15.4 ± 1.5	17.2 ± 0.5	22.1 ± 1.3

The compressive studies of 3D lattice structures indicated that lattices of types 1 and 2 deformed in a similar manner and had almost the same yield stresses (14.0–15.4 GPa). The layers deform almost uniformly or simultaneously with increasing stress. Small drops on the curves testify that some generatrixes located at 45° failed.

The strength properties of the lattices are summarized in Table 2.

The 3D lattices of type 2 behave differently when compressed (Fig. 9). In particular, such samples deform layer by layer since the cell generatrixes are located at 90°. Accordingly, the components degrade discretely: layer one deforms first, then layer two, and so on.

Table 2 shows only elastic limits and yield stresses since the materials are ductile and do not fail under such testing in the classical sense; i.e., they do not break into parts and, therefore, it is not correct to indicate the yield stress of lattice structures with 80% pore volume. Note that the greatest elastic limit and yield stress are exhibited by the lattices of type 2, which is associated with layer-by-layer cell deformation.

Impact toughness testing of 3D lattice structures also showed that the lattices of type 2 had the greatest impact toughness and yield stress in compression and the elastic modulus (Table 2). The lowest impact toughness was observed for the lattice of type 1; the samples failed completely. The lattices of type 3 deform in a similar way as the lattices of type 2 do. This is attributed to the same cell orientation at the y axis, which corresponds to the

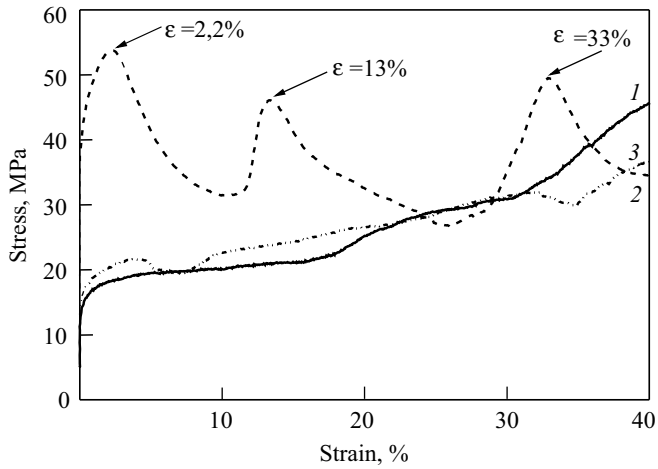

Fig. 9. Stress–strain curve for lattice structures in compression

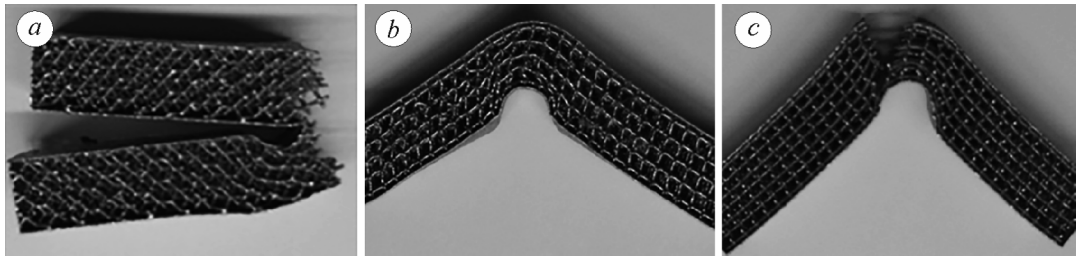

Fig. 10. Images of 3D lattices of types 1 (*a*), 2 (*b*), and 3 (*c*) after impact toughness testing

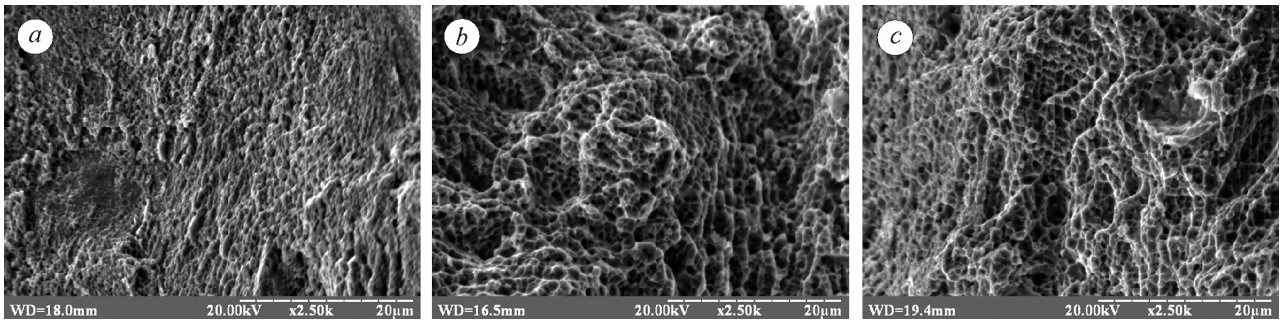

Fig. 11. Fracture patterns for 3D lattices of type 1 (*a*), 2 (*b*), and 3 (*c*) after impact toughness testing

pendulum movement, but different orientation of the cells at other axes leads to partial fracture of the lattices of type 3 (Fig. 10). The lattices of type 2 deform without fracture because the parallel location of cells to the *x*, *y*, and *z* axes ensures gradual deformation at impact. Hence, the configuration of cells in the lattices of type 2 promoted their high damping properties.

Analysis of fracture patterns for the samples after the lattices were tested by impact toughness indicated that the iron lattices of all three types were characterized by pit microrelief typical of viscous fracture (Fig. 11).

CONCLUSIONS

The effect of 3D lattice parameters, such as the orientation of unit cells as simple cubes, on the deformation of materials produced from iron powders by selective laser melting has been established.

The mechanical tests of lattice structures have shown that the orientation of unit cells in the material determines the elastic limits and yield stresses in compression and impact toughness. These properties differ for lattice types because their deformation differs: in the case of discrete (incremental) deformation of lattice generatrixes, the yield stress for the lattices of type 2 is 40.5–41.6 MPa, which is three times the yield stress of the lattices of types 1 and 3.

The simulated deformation of lattice structures with parallel-sided unit cells was confirmed by experimental studies. This testifies that the chosen methods are correct. In the future, the behavior of lattice structures should be assessed by simulating the deformation process using software packages that allow analyzing the complex orientation of unit cells located at different angles relative to the load applied.

ACKNOWLEDGMENTS

The authors are grateful to Director of the 3DMetalTech Company, Yaroslav Golovenko, for assistance in the printing of lattice structures.

REFERENCES

1. Pratheesh S. Kumar, S. Elangovan, R. Mohanraj, and J.R. Ramakrishna, “Review on the evolution and technology of State-of-the-Art metal additive manufacturing processes,” *Mater. Today: Proc*., **46**, Part 17, 7907–7920 (2021), https://doi.org/10.1016/j.matpr.2021.02.567.

2. Ahn. Dong-Gyu, “Direct metal additive manufacturing processes and their sustainable applications for green technology: A review,” *Int. J. Precis. Eng. Manuf. Green Technol*., **3**, 381–395 (2016).
3. G.K. Sujan, Huijun Li, Zengxi Pan, Daniel Liang, and Nazmul Alam, “Microstructural characterization and oxidation performance of solution-annealed and precipitation hardened wire-arc additively manufactured Inconel 718 superalloys,” *Addit. Manuf*., **51**, 102608 (2022), https://doi.org/10.1016/j.addma.2022.102602.
4. S.L. Taylor, A.E. Jakus, R.N. Shah, and D.C. Dunand, “Iron and nickel cellular structures by sintering of 3D-printed oxide or metallic particle inks,” *Adv. Eng. Mater.*, 1–8 (2016), DOI: 10.1002/adem.201600365.
5. P. Platek, J. Sienkiewicz, J. Janiszewski, and F. Jiang, “Investigations on mechanical properties of lattice structures with different values of relative density made from 316L by selective laser melting (SLM),” *Materials (Basel)*, **13**, No. 9, 2204 (2020), DOI: 10.3390/ma13092204.
6. L.E. Murr, E. Martinez, K.N. Amato, S.M. Gaytan, J. Hernandez, P.W. Shindo, F. Medina, and R.B. Wicker, “Fabrication of metal and alloy components by additive manufacturing: examples of 3D materials science,” *J. Mater. Technol*., **1**, No. 1, 42–54 (2012).
7. Z. Alomar and F. Concli, “A review of the selective laser melting lattice structures and their numerical models,” *Adv. Eng. Mater.*, 2000611, 1–17 (2020), DOI: 10.1002/adem.202000611.
8. Ajit Panesar, Meisam Abdi, Duncan Hickmana, and Ian Ashcroft, “Strategies for functionally graded lattice structures derived using topology optimization for additive manufacturing,” *Addit. Manuf*., **19**, 81–94 (2018).
9. F. Bartolomeu, M.M. Costa, N. Alves, G. Miranda, and F.S. Silva, “Selective laser melting of Ti6Al4V sub-millimetric cellular structures: prediction of dimensional deviations and mechanical performance,” *J. Mech. Behav. Biomed. Mater*., **113**, 104123 (2021).
10. L.J. Gibson and M.F. Ashby, *Cellular Solids*: *Structure and Properties*, 2nd ed., Cambridge University Press, Cambridge (2014).
11. M. Bici, S. Brischetto, F. Campana, C.G. Ferro, C. Seclì, S. Varetti, P. Maggiore, and A. Mazza, “Development of a multifunctional panel for aerospace use through SLM additive manufacturing,” in: *Proc. 11th CIRP Conference on Intelligent Computation in Manufacturing Engineering*. *Procedia CIRP 67*, 215–220 (2018), doi:10.1016/j.procir.2017.12.202.
12. Recep Gumruk, R.A.W. Mines, and Sami Karadeniz, “Static mechanical behaviors of stainless steel micro-lattice structures under different loading conditions,” *Mater. Sci. Eng. A*., **586**, 392–406 (2013).
13. Li Chuanlei, Lei Hongshuai, Liu Yabo, Zhang Xiaoyu, Xiong Jian, Zhou Hao, and Fang Daining, “Crushing behavior of multi-layer metal lattice panel fabricated by selective laser melting,” *Int. J. Mech. Sci*., **145**, 389–399 (2018).
14. C.G. Ferro, S. Varetti, P. Maggiore, M. Lombardi, S. Biamino, D. Manfredi, and F. Calignano, “Design and characterization of trabecular structures for an anti-icing sandwich panel produced by additive manufacturing,” *J. Sandwich Struct. Mater*., **22**, No. 4, 1111–1131 (2020), DOI: 10.1177/1099636218780513.
15. Kwang-Min Park, Kyung-Sung Min, and Young-Sook Roh, “Design optimization of lattice structures under compression: study of unit cell types and cell arrangements,” *Materials*, **15**, 97 (2022), https://doi.org/10.3390/ma15010097.
16. P.I. Loboda, A.V. Minitski, E.G. Biba, M.O Sysoev, and S.V. Radchuk, “Effect of the porous skeletal iron structure on the infiltration of aluminum melts,” *Powder Metall. Met. Ceram.*, **58**, No. 11–12, 651–656 (2020).
17. M. Gouge, “The finite element method for the thermo-mechanical modeling of additive manufacturing processes,” in: P. Michaleris (ed.), *Thermo-Mechanical Modeling of Additive Manufacturing*, Butterworth–Heinemann, Oxford, UK (2018).
18. I. Koutiri, E. Pessard, P. Peyre, O. Amlou, and T. de Terris, “Influence of SLM process parameters on the surface finish, porosity rate and fatigue behavior of as-built Inconel 625 parts,” *J. Mater. Process. Technol*., **255**, 536–546 (2018).